ACS APPLIED NANO MATERIALS

www.acsanm.org Article

Bright-Dark Exciton Interplay Evidenced by Spin Polarization in CdSe/CdMnS Nanoplatelets for Spin-Optronics

Elena V. Shornikova,* Dmitri R. Yakovlev,* Danil O. Tolmachev, Mikhail A. Prosnikov, Peter C. M. Christianen, Sushant Shendre, Furkan Isik, Savas Delikanli, Hilmi Volkan Demir, and Manfred Bayer

Cite This: *ACS Appl. Nano Mater.* 2025, 8, 974−984 Read Online

ACCESS | Metrics & More | Article Recommendations | Supporting Information

ABSTRACT: Diluted magnetic semiconductor (DMS) colloidal nanocrystals demonstrate remarkable magneto-optical properties. The ability to control their magnetization and, consequently, the circular polarization of exciton emission holds significant potential for spintronic applications. However, the interplay between bright and dark exciton recombination and its impact on the polarization of emission are not yet fully understood. We measure the magneto-optical properties of colloidal CdSe/CdMnS nanoplatelets at cryogenic temperatures in high magnetic fields up to 30 T. The degree of circular polarization of photoluminescence demonstrates nonmonotonous behavior in a magnetic field. In low magnetic fields, the polarization degree is positive due to an exchange interaction of excitons with localized spins of magnetic Mn^{2+} ions. After reaching a maximum, the polarization degree starts to decrease and reverses the sign to negative in high magnetic fields, which is unusual in DMSs. The critical magnetic field, in which the sign is reversed, increases when the temperature is elevated. We develop a model that explains this behavior by an interplay of bright and dark exciton recombination. In high magnetic fields, the dark exciton radiative recombination rate accelerates due to mixing with the bright state, and the intrinsic Zeeman splitting of dark exciton overcomes the exchange with Mn^{2+} ions. As a result, the lowest $|-2\rangle$ exciton energy level dominates in emission, providing negatively polarized photoluminescence.

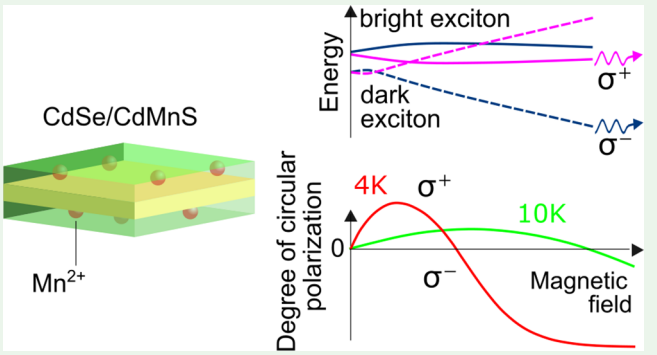

KEYWORDS: *diluted magnetic semiconductors, CdSe nanoplatelets, colloidal nanocrystals, magneto-optics, high magnetic fields*

Downloaded via BILKENT UNIV on January 20, 2025 at 07:28:06 (UTC).
See https://pubs.acs.org/sharingguidelines for options on how to legitimately share published articles.

1. INTRODUCTION

Diluted magnetic semiconductor (DMS) colloidal nanocrystals (NCs) are formed by doping colloidal NCs with transition-metal ions; commonly Mn^{2+} ions are used for II−VI semiconductors.[1−3] The strong exchange interaction between the host semiconductor *sp*−electrons and holes, and the localized transition-metal *d*−electrons, leads to bright spin-dependent and magneto-optical phenomena, such as giant Zeeman splitting,[4] giant Faraday and Kerr rotation,[5] and magnetic polaron formation.[6−8] These phenomena were first investigated in bulk DMS materials based on II−VI semiconductors like (Cd,Mn)Te, (Zn,Mn)Se, and so forth, and later in DMS quantum wells and quantum dots grown by molecular-beam epitaxy.[9−13]

Colloidal DMS NCs, due to their tunable properties, are promising for diverse applications ranging from spintronics and quantum technologies[14−18] to optoelectronics[19,20] and biomedical imaging.[21−24] Their unique ability to combine magnetism with optical properties makes them versatile components for future technological innovations.

The synthesis and understanding of optical properties of colloidal DMS NCs are still at an early stage, while several important results have already been established. Giant Zeeman splitting has been demonstrated in various experiments.[25−30] In contrast to intrinsic Zeeman splitting, which is observed in nonmagnetic NCs, the exchange interaction with magnetic impurities provides an additional spin splitting, which can be several orders of magnitude larger than the intrinsic splitting. The exchange interaction of excitons with Mn^{2+} ions has been proven by optically detected magnetic resonance (ODMR),[31−33] as well as high-frequency electron paramagnetic resonance (EPR) and electron nuclear double resonance (ENDOR).[34] Magnetic polaron formation has

Received: September 18, 2024
Revised: December 16, 2024
Accepted: December 18, 2024
Published: January 8, 2025

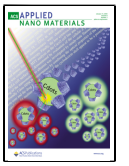

ACS Publications © 2025 American Chemical Society

https://doi.org/10.1021/acsanm.4c05364
ACS Appl. Nano Mater. 2025, 8, 974−984

been published,[35,36] and giant internal magnetic fields due to Mn spin fluctuations have been reported.[37]

In particular, DMS two-dimensional colloidal nanoplatelets (NPLs) are interesting because NPLs have extraordinary optical properties compared to spherical NCs and nanorods.[38] They inherit from nonmagnetic NPLs high quantum yields, narrow emission spectra, fast radiative recombination times, and possibility to control their structure on a monolayer scale.[39−48] The most studied DMS NPLs have CdSe cores and doped CdMnS shells.[29,42,49,50] In these structures, the electrons and holes are confined in the nonmagnetic CdSe core, and the penetration of their wave functions into the CdMnS shells provides the *sp*−*d* exchange interactions. CdMnS NPLs with strong overlap of the carrier wave function with Mn^{2+} ions have also been synthesized,[51] and silver-doped CdSe NPLs have demonstrated magnetic behavior.[52]

Photoluminescence (PL) of excitons in DMS CdSe-based quantum dots is found only if the exciton energy is below the Mn emission at 2.1 eV, which is valid only for large-size NCs.[27,53] CdSe/CdMnS NPLs do not demonstrate Mn emission,[29,42] probably due to limited penetration of electron and hole wave functions into the shells,[29,42,50] which is strong enough for *sp*−*d* exchange but not sufficient for effective energy transfer from excitons to Mn. Also, double, exciton and Mn, emission has been reported in ZnSe:Mn-based NCs with a large separation between exciton and Mn emission energies.[54−56]

There is a very limited number of studies on the polarized emission of excitons in high magnetic fields in DMS colloidal NCs. CdSe-based quantum dots[27,57] and NPLs[42,52] have been studied in magnetic fields up to 5 T, demonstrating a rapid increase and saturation of the degree of circular polarization (DCP). Among other materials, Mn-doped PbS colloidal quantum dots have been measured up to 30 T.[28] We have previously reported on magneto-optical studies of DMS NPLs in magnetic fields up to 15 T.[29] A rapid increase in DCP, followed by a slow decrease, was observed.

In this article, we study the magneto-optical properties of core/shell CdSe/CdMnS NPLs, which arise from excitons interacting with magnetic Mn^{2+} ions. Experiments are performed in high magnetic fields up to 30 T and at cryogenic temperatures down to 4 K. A nonmonotonous dependence of the DCP of PL on the magnetic field is found. We demonstrate that the interplay between dark and bright exciton states is responsible for this behavior and develop a model that qualitatively describes the experimental results.

2. EXPERIMENTAL SECTION

2.1. Sample Preparation. *2.1.1. Chemicals.* Cadmium acetate dihydrate ($Cd(OAc)_2{\cdot}2H_2O$), trioctylamine (TOA), oleylamine (OLA), *N*-methylformamide (NMF), ammonium sulfide solution (40−48 wt % in water), trioctylphosphine (TOP), oleic acid (OA), hexane, acetonitrile, toluene, and manganese(II) acetate from Sigma-aldrich.

2.1.2. Synthesis of 2 ML CdSe Nanoplatelets. The synthesis of the NPLs was performed according to a previously reported method.[58] A mixture of 860 mg of $Cd(OAc)_2{\cdot}2H_2O$, 1 mL of OA, and 60 mL of TOA was degassed for 1 h at room temperature. Then, it was heated to 115 °C under an argon flow. When the temperature reached 115 °C, 1 mL of 1 M TOP-Se was swiftly injected, and the mixture was kept at 115 °C for 2 h. After that, the solution was cooled down to room temperature and centrifuged after the addition of ethanol and hexane. The precipitated NPLs were dispersed in hexane.

2.1.3. Synthesis of CdSe/CdMnS and CdSe/CdZnMnS Core/Shell NPLs. Here, we used a modified procedure of the c-ALD recipe reported previously.[59] The 2 ML CdSe NPLs were dispersed in 1 mL of hexane, and 5 mL of NMF with 40 μL of a 40−48% aqueous solution of ammonium sulfide—as the sulfur shell growth precursor—was added on top of the NPL dispersion and stirred for 2 min. Then, the reaction was stopped by the addition of acetonitrile and excess toluene, and the mixture was precipitated via centrifugation. The precipitate was redispersed in NMF and precipitated again after the addition of acetonitrile and toluene to remove unreacted precursors. Finally, the NPLs were dispersed in 4 mL of NMF. The cation precursor solution consisted of $Mn(OAc)_2$ and $Cd(OAc)_2{\cdot}2H_2O$ in NMF for the deposition of the CdMnS shell to obtain CdSe/CdMnS core/shell NPLs, and $Mn(OAc)_2$, $Cd(OAc)_2{\cdot}2H_2O$, and $Zn(OAc)_2{\cdot}2H_2O$ in NMF for the deposition of the CdZnMnS shell to obtain CdSe/CdZnMnS core/shell NPLs. For the cation deposition step, 1 mL of the cation precursor mixture was added to the NPL dispersion, and it was stirred for 45 min in a nitrogen-filled glovebox. Then, the reaction was stopped by the addition of excess toluene, and the mixture was precipitated via centrifugation and dispersed in NMF. The same cleaning step was repeated twice more to remove excess precursors. To increase the number of shells, the steps explained above were repeated until the desired shell thickness was achieved. Lastly, 5 mL of hexane and 100 μL of OLA were added on top of the precipitated NPLs after achievement of the desired shell thickness, and the mixture was stirred overnight. To remove excess ligands, the dispersion of NPLs was precipitated by addition of ethanol, redispersed, and kept in hexane for further usage.

Samples #1−#3 had cores synthesized in the same batch. Samples #2 and #3 were synthesized in the same c-ALD synthesis. This means that, after growing 2 ML shells on each side of the cores, a portion of the solution was taken to finish the synthesis and produce sample #2, while the rest was used to grow 4 ML thicker shells and produce sample #3.

Similarly, samples #4−#6 had the same cores and were synthesized together. After growing a 1 ML shell on each side of the CdSe cores, a portion of the NPLs was taken to produce sample #4. The rest was used to grow an additional shell of 1 ML, and after this procedure, a portion of the NPLs was taken to produce sample #5. The rest was taken to repeat growth of the 1 ML shell and used to produce sample #6.

2.2. Experiments in Magnetic Fields up to 30 T. The measurements were performed in the High Field Magnet Laboratory (HFML), Nijmegen. Samples were mounted on a titanium sample holder on top of a three-axis piezo-positioner. The sample stage was placed in an optical probe made of carbon and titanium to minimize possible displacements at high magnetic fields. Laser light was focused on the sample by a singlet objective (2 mm working distance). The same lens was used to collect the PL emission and direct it to the detection setup (backscattering geometry). The optical probe was mounted inside a liquid helium bath cryostat (4.2 K) inserted in a 50 mm bore Florida-Bitter electromagnet with a maximum *dc* magnetic field strength of 31 T. Experiments were performed in Faraday geometry (excitation and detection beams were parallel to the magnetic field direction).

The PL was excited by a diode laser operating at 405 nm (photon energy of 3.06 eV) in a continuous wave (cw) or pulsed mode (pulse duration of 40 ps). The PL was dispersed with a 0.3 m spectrometer and detected either by a liquid-nitrogen-cooled charge-coupled device (CCD) camera or a Si avalanche photodiode (APD) connected to a conventional time-correlated single-photon counting system. The instrumental response time was about 200 ps. The PL circular polarization degree was analyzed by a combination of a quarter-wave plate and a linear polarizer. The duration of the time-resolved measurements was limited to 1 min, which was the amount of time the magnet could stay in high magnetic fields. For this reason, the measured decay rates have a low accuracy, with an error of ±5 ns.

2.3. Lifetime Measurements. Recombination dynamics at temperatures down to 2 K were measured at TU Dortmund. The PL was excited by a diode laser operating at 405 nm (photon energy

https://doi.org/10.1021/acsanm.4c05364
ACS Appl. Nano Mater. 2025, 8, 974−984

Table 1. Parameters of the Studied CdSe/CdS and CdSe/CdMnS NPLs

sample	core thickness	shell thickness	total thickness	f_e (ΔE_c = 0.3 eV)	f_h (ΔE_v = 0.45 eV)	Mn concentration	emission energy (T = 4 K), eV
#1	2 ML	2 ML	6 ML	0.37	0.22	0	2.22
#2	2 ML	2 ML	6 ML	0.37	0.22	0.4%	2.21
#3	2 ML	6 ML	14 ML	0.58	0.26	0.4%	2.12
#4	4 ML	1 ML	6 ML	0.08	0.03	0.4%	2.13
#5	4 ML	2 ML	8 ML	0.18	0.06	0.4%	2.07
#6	4 ML	3 ML	10 ML	0.24	0.07	0.4%	2.01

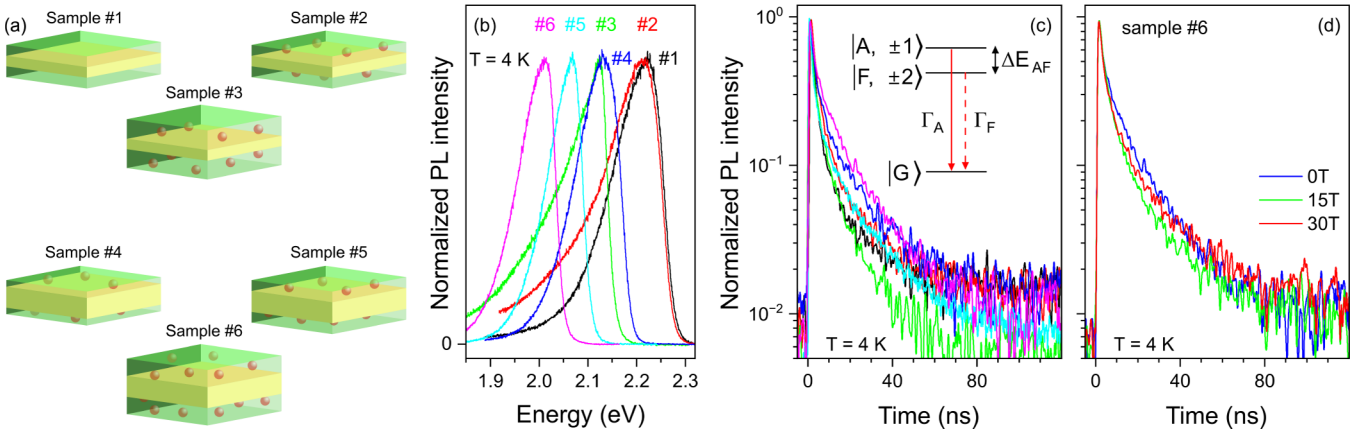

Figure 1. (a) Cartoons representing the studied NPL samples. Yellow layers: CdSe cores; green layers: CdS shells; red balls: Mn^{2+} ions. (b) Photoluminescence spectra of the samples at T = 4 K. (c) Recombination dynamics measured at the emission maxima. Color codes are the same as in panel (b). Inset presents the three-level model: $|A\rangle$ and $|F\rangle$ are the bright and dark exciton states, $|G\rangle$ is the unexcited crystal state, ΔE_{AF} is the bright-dark exciton splitting, Γ_A and Γ_F are the radiative recombination rates of bright and dark excitons, respectively. (d) Recombination dynamics in sample #6 measured at emission maximum in magnetic fields of 0, 15, and 30 T at T = 4 K.

of 3.06 eV) in pulsed mode (pulse duration of 40 ps). The PL was dispersed with a 0.5 m spectrometer and detected by a Si APD connected to a conventional time-correlated single-photon counting system. The instrumental response time was about 200 ps.

3. RESULTS AND DISCUSSION

Six CdSe/CdMnS and CdSe/CdS NPL samples were grown in this study. The synthesis was performed according to our previously published procedures (see refs 42,58,59 and the Section 2 for details). Samples #1−#3 have 2 ML (monolayer) thick CdSe cores and shells consisting of 2 ML of CdS (#1), 2 ML of CdMnS (#2), and 6 ML of CdMnS (#3) cladding the core. Samples #4−#6 have 4 ML thick CdSe cores and CdMnS shells with 1 ML (#4), 2 ML (#5), and 3 ML (#6) thicknesses.

Several studies, which we have performed before on similar samples, have confirmed the successful doping of Mn into the shells of the NPLs. First, as also observed in the present study, the circular polarization of emission in an external magnetic field reverses its sign, changing from negative in undoped NPLs to positive in Mn-doped NPLs. This behavior is attributed to the exchange interaction between charge carriers and magnetic Mn^{2+} ions.[29,42] Second, ODMR reveals a resonance, responsible for the interaction of excitons, localized in CdSe cores, with Mn^{2+} ions in CdMnS shells.[29,32] Third, successful Mn doping inside the lattice of CdS shells is confirmed by high-frequency EPR.[34]

Samples #2−#6 have similar Mn concentrations of about x = 0.004 (0.4%) according to our previous studies using ODMR on similar NPLs.[29,32] The sample parameters are given in Table 1, and cartoons representing the NPL structures are shown in Figure 1a.

Figure 1b shows PL spectra of all samples measured at T = 4 K. Samples #1 and #2 have similar core and shell thicknesses, but sample #2 has Mn in the shell. These two samples have very similar PL spectra with emission maxima at the energies of 2.22 and 2.21 eV, respectively. This shows that the implementation of a small Mn concentration does not change the exciton emission. Emission of sample #3 with the same core and a thicker shell is red-shifted to 2.12 eV due to the penetration of electron and hole wavefuctions into the shell, which reduces the quantization energies of the electrons and holes. Samples #4−#6 have similar cores with 4 ML thickness and shells increasing from 1 to 3 ML, and their emission maxima are at 2.13, 2.07, and 2.01 eV, with smaller energies corresponding to thicker shells. All six samples have fwhm (full width at half-maximum) of about 100 meV, which is typical for core/shell NPLs and is explained by the inhomogeneous broadening of the NPL ensembles and multiple emission lines from individual NPLs.[60,61]

Figure 1c shows recombination dynamics measured at emission maxima with a time resolution of 200 ps. All dynamics are quite similar; they are multiexponential with an initial fast decay on a time scale of about 3 ns followed by a slower decay. The average lifetimes estimated from three-exponential decays are from 15 to 40 ns with an error of ±5 ns (see the Section 2).

Figure 1d shows recombination dynamics measured at the emission maximum in sample #6 at various magnetic fields up to 30 T. The PL decays remain unchanged under an applied magnetic field. Additional data on emission decays in samples #1−#6 measured at various temperatures and magnetic fields are presented in Supporting Information S1.

https://doi.org/10.1021/acsanm.4c05364
ACS Appl. Nano Mater. 2025, 8, 974−984

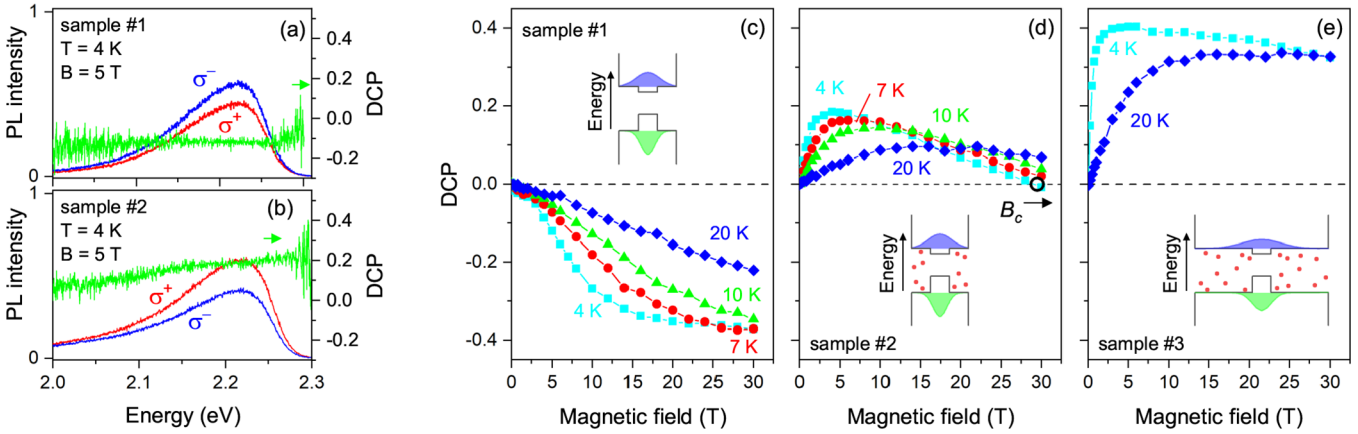

Figure 2. (a, b) Spectra of the σ^+ (red)- and σ^- (blue)-polarized PL in samples #1 and #2 measured at T = 4 K and B = 5 T. Right scale: spectrally resolved degree of circular polarization (DCP, green). (c–e) DCP measured at PL maximum as a function of the magnetic field at various temperatures: (c) sample #1, (d) sample #2, and (e) sample #3. Cartoons schematically show the band structures and electron and hole wave functions (blue and green contours, respectively).

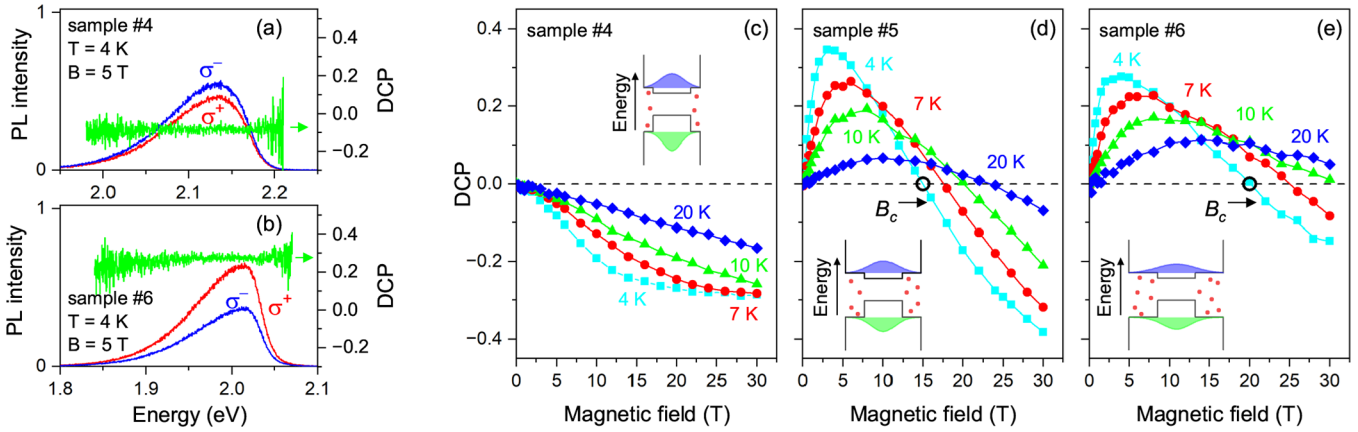

Figure 3. (a, b) Spectra of the σ^+ (red)- and σ^- (blue)-polarized PL in samples #4 and #6 measured at T = 4 K and B = 5 T. Right scale: spectrally resolved degree of circular polarization (DCP, green). (c–e) DCP measured at the PL maximum as a function of the magnetic field at various temperatures: (c) sample #4, (d) sample #5, and (e) sample #6. Cartoons schematically show the band structures and electron and hole wave functions (blue and green contours, respectively).

The exciton recombination dynamics in our samples are weakly affected by the temperature or magnetic field. We discussed this issue in similar samples in ref 29. In short, in CdSe-based core/shell NPLs, the exciton fine structure has five states, with the two lowest exciton states being the dark exciton $|F\rangle$ with the angular momentum projections $|\pm 2\rangle$ and the bright exciton $|A\rangle$ with the angular momentum projections $|\pm 1\rangle$[41,62,63] (see inset in Figure 1c). The other three states, with angular momentum projections $|0^L\rangle$, $|\pm 1^U\rangle$, and $|0^U\rangle$, are separated by more than 100 meV from the $|A\rangle$ and $|F\rangle$ states and do not participate in emission. The splitting between the $|A\rangle$ and $|F\rangle$ states, ΔE_{AF}, is typically about 1 meV in similar NPLs,[29,64] which is comparable to k_BT even at cryogenic temperatures. Here, k_B is the Boltzmann constant. Excitons populate both the dark and bright exciton states. The dark state has a higher occupation than the bright state, but its radiative recombination rate is slower: $\Gamma_F < \Gamma_A$, and the emission is contributed by the dark and bright excitons. Here, Γ_F and Γ_A are the radiative recombination rates of the dark and bright excitons, respectively. As a result, the PL dynamics are not sensitive to changes of the magnetic field and temperature, as is the case in colloidal bare CdSe NPLs and NCs with large bright-dark splittings.[41,63,65−67] The magnetic field, on one hand, splits the exciton energy levels, which leads to the thermal redistribution of exciton populations of these levels. On the other hand, the magnetic field mixes the bright and dark exciton states, accelerating the dark exciton and slowing down the bright exciton radiative rates. It should be noted that the acceleration only occurs for NPLs with the quantization axis tilted relative to the magnetic field direction, but this is true for most NPLs in the ensemble (see Supporting Information S1). Our experimental accuracy of measuring radiative recombination rates is about ±30% (see the Section 2), and we cannot resolve small variations of the rate.

It should be noted that the PL dynamics, which are not affected by temperature and magnetic field, could indicate trion (charged exciton) recombination. However, we are convinced that excitons are the main emitting states in these NPLs for two reasons: (i) exciton emission has been reported in various core/shell CdSe/CdS NPLs with thin shells,[29,31,64] and (ii) trion emission would not explain the nonmonotonous dependence of the DCP on a magnetic field (see below). It is possible that trion emission also has some impact on the PL. Taking trions into account would not change the results but would complicate the modeling. Therefore, we consider only exciton emission and neglect the trions.

https://doi.org/10.1021/acsanm.4c05364
ACS Appl. Nano Mater. 2025, 8, 974−984

Figure 2a,b shows circularly polarized PL spectra of samples #1 and #2 measured at $T = 4$ K in a magnetic field of $B = 5$ T. The spectra are normalized so that the intensity of the sum of σ^+ and σ^--polarized PL at the emission maximum equals unity. In nonmagnetic sample #1, the σ^--polarized PL has larger intensity, while in DMS sample #2, the σ^+-polarized PL is stronger. The DCP is calculated using the following equation:

$$\mathrm{DCP} = \frac{I^+ - I^-}{I^+ + I^-} \tag{1}$$

where I^+ and I^- are the intensities of σ^+- and σ^--polarized PL, respectively. In sample #1, the DCP is negative and equals −0.1, while in sample #2, the DCP is positive and equals +0.2. In all studied samples, the spectral dependence of the DCP is weak or absent.

Figure 2c−e shows the DCP in samples #1−#3 measured at various temperatures in magnetic fields from 0 to 30 T. In sample #1 at 4 K, the absolute DCP value increases in $B < 10$ T and starts to saturate in $B > 10$ T, reaching −0.36 in high magnetic fields. At higher temperatures, the absolute DCP value increases slowly with the magnetic field, and at 20 K, the DCP cannot reach saturation. In sample #2 at 4 K, the DCP depends on the magnetic field nonmonotonously. Initially, it is positive and reaches +0.18 at $B = 5$ T. In stronger fields, the DCP decreases and crosses zero at a critical magnetic field $B_c = 29.5$ T. When the temperature increases, the DCP maximum value reduces, and B_c shifts to higher magnetic fields, which cannot be reached in our experiments. Sample #3 has a positive DCP, which reaches +0.4 already at $B = 3$ T at 4 K, and slightly decreases in higher magnetic fields. At 20 K, the DCP saturates at +0.33 for $B > 10$ T.

Qualitatively similar behavior is found in samples #4−#6. Figure 3a,b shows polarized PL spectra of samples #4 and #6 at $B = 5$ T. In sample #4, the DCP is negative and equals −0.08, while in sample #6, it is positive and equals +0.28. Figure 3c−e shows the DCP in samples #4−#6 at various temperatures measured in magnetic fields from 0 to 30 T. In sample #4 at 4 K, the DCP monotonously reaches the saturation value of −0.29 at $B = 30$ T. At higher temperatures, the absolute DCP value increases slowly with field growth, and at 20 K, the DCP cannot reach saturation. Surprisingly, despite the presence of Mn^{2+} in sample #4, its DCP is negative and shows behavior similar to the nonmagnetic sample #1, compare with Figure 2c, which indicates the very weak interaction of excitons with the Mn^{2+} ions in this sample with a thin CdMnS core. In samples #5 and #6, the DCP is nonmonotonous. In sample #5 at 4 K, it reaches +0.35 at $B = 3.5$ T, crosses zero at $B_c = 15$ T, and reaches −0.38 at $B = 30$ T, still not saturating. At higher temperatures, B_c shifts to higher fields, reaching $B_c = 24$ T at 20 K. In sample #6, the behavior is similar, but B_c is slightly higher: $B_c = 20$ T at 4 K, and more than 30 T at 20 K.

The DCP dependence on the magnetic field in samples #1 and #4 is typical for CdSe-based nonmagnetic colloidal NCs,[65,68,69] but the DCP observed in other samples is unusual. There are two experimental facts that have to be explained. First, a nonmonotonous DCP dependence on a magnetic field, and second, an increase of B_c with increasing temperature.

Three mechanisms could be responsible for this (i) interplay between the intrinsic and exchange Zeeman splittings of excitons or trions, (ii) spin-dependent recombination of dark excitons, and (iii) interplay between bright and dark exciton states emitting in σ^+ and σ^- polarizations, respectively. Let us consider these mechanisms. We use the conventional approach for diluted magnetic semiconductors, which is based on the consideration of the exchange interaction of an exciton with the Mn^{2+} ions within the mean-field approximation.[10,12] Recently, we successfully implemented this approach to describe the DCP in CdSe/CdMnS NPLs.[29,42]

3.1. Interplay between the Intrinsic and Exchange Zeeman Splittings of Excitons or Trions. The exchange interaction of electron band states with localized magnetic ions results in giant Zeeman splitting. The Zeeman splitting of electrons, holes, or excitons in DMS materials has two contributions:

$$\Delta E_Z(B) = \Delta E_Z^{\mathrm{intr}}(B) + \Delta E_Z^{\mathrm{exch}}(B) \tag{2}$$

Here, $\Delta E_Z^{\mathrm{intr}}(B)$ is the intrinsic Zeeman splitting characteristic for nonmagnetic NCs. In the presence of an external magnetic field $\vec{B}$, a particle with a magnetic moment $\vec{\mu}$ acquires an energy $\Delta E_Z^{\mathrm{intr}}(B) = -\vec{\mu}\cdot\vec{B}$. The magnetic moment can be expressed as $\vec{\mu} = g\mu_B\vec{J}$, where g is the g-factor, μ_B is the Bohr magneton, and $\vec{J}$ is the angular momentum of the particle. The energies acquired by, for example, bright exciton states with angular momentum projections $J_Z = |-1\rangle$ and $J_Z = |+1\rangle$ are different, and a Zeeman splitting between these two states appears. $\Delta E_Z^{\mathrm{exch}}(B)$ represents the exchange energy due to the interaction of excitons or charge carriers with magnetic Mn^{2+} ions.

The Zeeman splitting of electrons in CdSe/CdMnS NPLs is

$$\begin{aligned}\Delta E_{Z,e}(B) &= \Delta E_{Z,e}^{\mathrm{intr}}(B) + \Delta E_{Z,e}^{\mathrm{exch}}(B)\\ &= g_e\mu_B B - \langle S_{Mn}(B)\rangle x N_0 \alpha f_e\end{aligned} \tag{3}$$

and of holes:

$$\begin{aligned}\Delta E_{Z,h}(B) &= \Delta E_{Z,h}^{\mathrm{intr}}(B) + \Delta E_{Z,h}^{\mathrm{exch}}(B)\\ &= -3g_h\mu_B B - \langle S_{Mn}(B)\rangle x N_0 \beta f_h\end{aligned} \tag{4}$$

Here, g_e and g_h are the electron and hole g-factors, respectively, $\langle S_{Mn}(B)\rangle$ is the mean spin of Mn^{2+} ions, x is the Mn concentration, N_0 is the number of cations per unit volume, α and β are the $s-d$ and $p-d$ exchange constants, respectively. f_e and f_h are the probabilities of finding an electron and a hole in the shells, respectively. Here, we assume that the heavy hole is the ground hole state, which is true for CdSe-based NPLs.[41,63] We use the definition of the hole g-factor sign that is commonly used for colloidal NCs.[70,71]

In the studied samples, the Mn^{2+} ions are located in the shells, and the penetration of the electron and hole wave functions into the shells controls the exchange interaction. The penetration can be calculated using a particle-in-a-box model (see Supporting Information S3). Since the conduction and valence band offsets between CdSe and CdS are not precisely known, the probabilities of finding an electron and a hole in the shell can be estimated with certain tolerance. The values of f_e and f_h, which we used for calculations of the DCP, are given in Table 1. The electron and hole wave functions are shown schematically in the insets of Figures 2c−e and 3c−e.

According to eqs 3 and 4, the exchange part of the carrier Zeeman splitting depends on the mean spin of the Mn^{2+} ions $\langle S_{Mn}(B)\rangle$. The dependence of $\langle S_{Mn}(B)\rangle$ on the magnetic field is described by the modified Brillouin function for spin 5/2 (see Supporting Information S4). Examples of calculated intrinsic and exchange electron and hole Zeeman splittings at

https://doi.org/10.1021/acsanm.4c05364
ACS Appl. Nano Mater. 2025, 8, 974−984

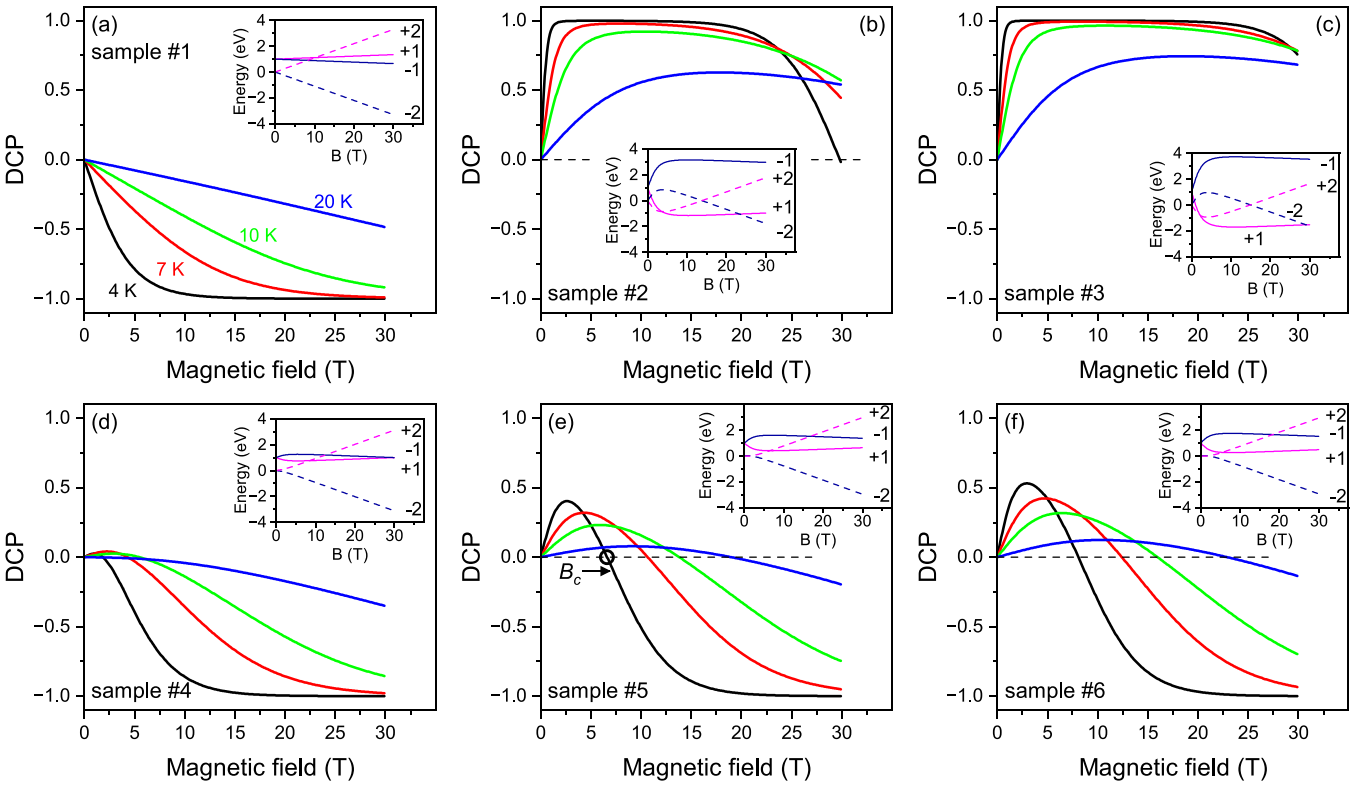

Figure 4. Calculated degree of circular polarization (DCP) of excitons as a function of the magnetic field at various temperatures for samples #1−#6 (panels (a−f), respectively) with parameters given in text. Insets show calculated exciton energies at T = 4 K; the σ^- emitting states are dark blue, and the σ^+ emitting states are pink.

various temperatures are shown in Figures S9 and S10. The exchange part increases rapidly in low magnetic fields and saturates for $B > 10$ T, while the intrinsic part increases linearly with the magnetic field. This means that, if the intrinsic and exchange splittings have opposite signs, there is a finite magnetic field B_c, in which $\Delta E_Z^{intr}(B_c) + \Delta E_Z^{exch}(B_c) = 0$. In this field, the Zeeman splitting reverses sign, and so does the DCP.

The competition between intrinsic and exchange splittings can explain the nonmonotonous dependence of the DCP on the magnetic field. This is valid for negatively charged trions and excitons but not for positively charged trions, which are not expected to demonstrate a nonmonotonous DCP, since their intrinsic and exchange splittings have the same signs. However, this competition does not explain the shift of the critical magnetic field B_c to higher fields with increasing temperature. Indeed, the average spin of Mn^{2+} ions decreases with increasing temperature, and consequently, the exchange splitting reduces. This means that the intrinsic splitting compensates for the exchange splitting at lower fields as the temperature increases, or, in other words, B_c decreases with increasing temperature. This is valid for any two-level system including negatively charged trions, dark excitons, and bright excitons (see Supporting Information S4 and S5 for more details).

3.2. Spin-Dependent Dark Exciton Recombination. A nonmonotonous dependence of the DCP on the magnetic field, with the sign reversal from positive to negative, has been observed in nonmagnetic bare-core CdSe NPLs.[72] The effect is caused by the spin-dependent recombination of the dark exciton, assisted by flips of the surface spins. The surface spins are polarized by the magnetic field, making the emission of excitons with an angular momentum projection $|+2\rangle$, which is σ^+-polarized, more favorable than the emission of excitons with an angular momentum projection $|-2\rangle$, which is σ^--polarized. In low magnetic fields, this effect can overcome the polarization caused by the thermal population of the Zeeman levels. In other words, while the exciton state with momentum projection $|-2\rangle$ has lower energy and higher occupation, the emission from the upper $|+2\rangle$ state is stronger due to the spin-dependent recombination via surface spins. When the magnetic field increases, the Zeeman splitting grows, and the occupation of the $|-2\rangle$ state increases. This is favorable for the σ^--polarized emission. Therefore, the DCP is positive in low magnetic fields and reverses the sign to negative in high magnetic fields. Under certain conditions, B_c increases with increasing temperature.

In core/shell NPLs, which are used in the present study, electron and hole wave functions are mostly localized in the cores and partly penetrate into the shells, but their amplitudes at the surface are very small compared to those of bare-core NPLs. Moreover, the surface spin-dependent recombination is not connected to the presence of Mn, and it would manifest itself in the nonmagnetic sample #1; however, a positive DCP is observed only in DMS samples. Therefore, we exclude the spin-dependent recombination assisted by surface spins from possible explanations of the nonmonotonous DCP.

The localized spins of magnetic Mn^{2+} ions can act for spin-dependent recombination similar to surface spins. We modeled a situation where only the dark exciton is involved in recombination, and the increase of B_c with increasing temperature is explained by strong Mn-assisted spin-dependent recombination process (see Supporting Information S7 for

https://doi.org/10.1021/acsanm.4c05364
ACS Appl. Nano Mater. 2025, 8, 974−984

more details). However, this hypothesis requires extremely strong Mn-assisted recombination with a rate four times faster than that of Γ_F. This would result in much faster PL dynamics in DMS NPLs compared to nonmagnetic sample #1, which is not observed experimentally (Figure 1c). We also did not observe such strong recombination acceleration in our previous studies on similar NPLs.[29]

The requirement for very strong Mn-assisted recombination is partially due to the fact that the recombination of dark excitons not assisted by Mn would lead to B_c shifting to lower fields with increasing temperature (see (Section 3.1)). The spin-dependent recombination should be very strong to compensate this effect.

With the arguments given above, we exclude spin-dependent recombination as the explanation of the increase of B_c with increasing temperature.

3.3. Interplay between Bright and Dark Exciton States Emitting in σ^+ and σ^- Polarizations, Respectively.

The bright exciton Zeeman splitting is calculated using the electron and hole splittings:

$$\Delta E_{Z,XA}(B) = g_{XA}\mu_B B + \Delta E^{exch}_{Z,XA}(B) \quad (5)$$

where $g_{XA} = -g_e - 3g_h$ is the bright exciton g-factor,[62,73] and $\Delta E^{exch}_{Z,XA}(B) = -\Delta E^{exch}_{Z,e} + \Delta E^{exch}_{Z,h}$ is the exchange term. Similarly, the dark exciton Zeeman splitting reads as

$$\Delta E_{Z,XF}(B) = g_{XF}\mu_B B + \Delta E^{exch}_{Z,XF}(B) \quad (6)$$

where $g_{XF} = g_e - 3g_h$ is the dark exciton g-factor,[62,73] and $\Delta E^{exch}_{Z,XF}(B) = \Delta E^{exch}_{Z,e} + \Delta E^{exch}_{Z,h}$ is the exchange term.

Figure 4 shows the modeled DCP at various temperatures in all samples. The insets show the corresponding energy levels of the bright and dark excitons as functions of the magnetic field at $T = 4$ K. The following parameters are used: $g_e = 1.7$,[29,74,75] $g_h = -0.7$,[67] $N_0\alpha = 0.22$ eV and $N_0\beta = -1.8$ eV,[12] $\Delta E_{AF} = 1$ meV,[29,64] f_e and f_h listed in Table 1, $\Gamma_A = 0.1$ ns^{-1}, and $\Gamma_F = 0.01$ ns^{-1} (see Supporting Information S1). Details of the modeling can be found in Supporting Information S4, S5.

The intrinsic dark and bright exciton g-factors are positive (+3.8 and +0.4, respectively). Therefore, in the nonmagnetic sample #1, the state with $|-2\rangle$ angular momentum projection has lower energy than the $|+2\rangle$ state, and the $|-1\rangle$ state has lower energy than the $|+1\rangle$ state (inset in Figure 4a). The intrinsic dark exciton splitting is larger than the intrinsic bright exciton splitting, compare the energy separation between the $|-2\rangle$ and $|+2\rangle$ states with the splitting between the $|-1\rangle$ and $|+1\rangle$ states. We neglect the anticrossing of exciton energy levels in our calculations because we observe no indication of it (sharp resonances in the dependences of total PL intensity and DCP on a magnetic field[76]), see Supporting Information S6 for more details.

The PL from sample #1 is σ^--polarized in a magnetic field (Figure 4a). At $T = 4$ K, it is mostly contributed by emission from the $|-2\rangle$ exciton state. At higher temperatures, the polarization degree decreases because the other states are thermally populated and participate in emission. In modeling, we assume the Boltzmann exciton distribution. It should be noted that we do not take into account the depolarizing factors so that the absolute value of the DCP at low temperatures and in high magnetic fields reaches 1 (i.e., 100%). In real NCs, various factors can reduce the polarization: orientation of the NPL quantization axis arbitrary to the magnetic field,[70,72] dynamical factor,[77] phonon-assisted recombination,[69,78] and linearly polarized emission due to the NPL anisotropic shape.[79] The dynamical factor is about unity in the studied samples (Figure S3); in other words, the spin relaxation time is small compared to the lifetime. We believe that NPL orientation (see Supporting Information S1) and linearly polarized emission due to the NPL shape are the main depolarization mechanisms. The absolute values of the DCP experimentally measured in this study do not exceed 0.4. Therefore, our calculations reproduce the shape, but not the absolute values.

Sample #2 (Figure 4b) has the same design as sample #1, but the shell is doped with Mn. The exchange interaction alters the energies of the exciton states in a magnetic field. The bright exciton $|+1\rangle$ state is lower than the $|-1\rangle$ state, and the splitting between them quickly increases with growing field and saturates at about 5 T. For the dark exciton, the exchange Zeeman splitting also inverts the $|\pm2\rangle$ states in low magnetic fields so that the $|+2\rangle$ state has lower energy. However, in magnetic fields above 14 T, the intrinsic splitting of the dark exciton dominates, and the $|-2\rangle$ dark exciton state is below the $|+2\rangle$ state. Above 23 T, the lowest exciton state is $|-2\rangle$. The corresponding DCP (black line in Figure 4b) is positive and reverses sign at 30 T. The magnetic field, in which the sign is reversed, is determined by the competition between the emission of the thermally populated $|-2\rangle$ and $|+1\rangle$ states. At higher temperatures, the $|+1\rangle$ level is populated in magnetic fields up to 30 T, and the DCP is positive (red, green, and blue lines in Figure 4b).

Sample #3 (Figure 4c) has a thicker shell and larger exchange energy. The $|+2\rangle$ state below 2 T and $|+1\rangle$ state above 2 T are the lowest in energy, and the emission is σ^+-polarized. At 4 K, the DCP saturates already at 1 T and stays at this nearly saturated level up to 30 T. At 20 K, the DCP increases in magnetic fields from 0 to 15 T and stays about constant above 15 T.

Sample #4 (Figure 4d) has a 4 ML thick core and 1 ML thick CdMnS shells. Due to the very small penetration of the electron and hole wave functions into the shell (Table 1), the exchange Zeeman splittings are very small. In the bright exciton, the exchange splitting slightly overcomes the intrinsic splitting, and the $|+1\rangle$ state has slightly lower energy than the $|-1\rangle$ state. In the dark exciton, the intrinsic splitting overcomes the exchange splitting, and the lowest dark exciton state is $|-2\rangle$. As a result, at 4 K the DCP is positive in low magnetic fields due to the dominating emission from the $|+1\rangle$ state and reverses the sign already at 2 T. In the experiment, we observed negative DCP starting from 0 T (compare with Figure 3c). At higher temperatures, the stronger contributions from the upper states reduce the DCP, but the behavior is generally the same.

Samples #5 and #6 (Figure 4e,f) have 2 and 3 ML thick shells, respectively. The penetrations of the electron and hole wave functions into the shells are stronger than in sample #4, which increases the exchange with Mn^{2+}. As we discussed above, the bright exciton has about an order of magnitude smaller intrinsic Zeeman splitting than the dark exciton because of the different g-factors. Additionally, the bright exciton has a larger exchange Zeeman splitting than the dark exciton because the electron exchange energy $\Delta E^{exch}_{Z,e}$ enters eqs 5 and 6 with opposite signs. As a result, the exchange with Mn^{2+} spins affects the bright exciton more strongly than the

https://doi.org/10.1021/acsanm.4c05364
ACS Appl. Nano Mater. 2025, 8, 974−984

dark exciton. The $|+1\rangle$ bright exciton state is always below the $|-1\rangle$ state, while in the dark exciton, the intrinsic splitting overcomes the exchange at 1.5 and 2 T in samples #5 and #6, respectively, at 4 K. In low magnetic fields at 4 K, the emission is σ^+-polarized because the $|+1\rangle$ bright exciton level is populated, and it has faster recombination rate. With the increasing magnetic field, the splitting between the lowest $|-2\rangle$ and the upper $|+1\rangle$ levels increases, and above about 6 T in sample #5 (8 T in sample #6), when only the $|-2\rangle$ level is populated, the DCP is σ^--polarized. At higher temperatures, stronger magnetic fields are needed to depopulate the $|+1\rangle$ level, and the critical magnetic field B_c shifts to higher fields.

Comparison of the modeling with experimental data indicates that the interplay between the bright and dark exciton states emitting in opposite polarizations can explain both the nonmonotonous dependence of the DCP on the magnetic field and the increase of the critical magnetic field B_c with increasing temperature.

We believe that a similar effect can be observed in various DMS and some nonmagnetic colloidal NCs. We found a similar behavior in CdSe/CdZnMnS NPLs (see Supporting Information S2). According to our calculations, NCs with a small bright-dark splitting and opposite signs of $\Delta E_{Z,XA}$ and $\Delta E_{Z,XF}$ are good candidates to observe this bright-dark exciton interplay (Supporting Information S8). The bright-dark splitting ΔE_{AF} is an important parameter, which should not exceed several meV; otherwise, the temperature population of the bright state would be too low. We predict that a similar interplay can be observed in nonmagnetic NCs with $g_e = 1.7$ and $g_h = -0.2$, and in large-size DMS quantum dots, where exciton emission is not quenched and ΔE_{AF} is small.

4. CONCLUSIONS

In summary, magneto-optical experiments on CdSe/CdMnS nanoplatelets reveal a strong influence of the exchange of excitons with Mn^{2+} ions on the circular polarization of PL. The competition between the bright and dark exciton PL leads to a nonmonotonous dependence of the degree of circular polarization on the magnetic field strength. The electron and hole exchange interactions with Mn^{2+} ions can be tuned by modifying the composition of nanoplatelets (material and thickness of core and shell layers, number of shells, and Mn concentration). This can be done with high precision since nanoplatelets are grown layer by layer. This makes them unique among the whole family of colloidal DMS nanocrystals. This flexibility can be used to reveal new spin-dependent effects in DMS colloidal nanocrystals.

■ ASSOCIATED CONTENT

Supporting Information

The Supporting Information is available free of charge at https://pubs.acs.org/doi/10.1021/acsanm.4c05364.

Additional experimental data: time-resolved measurements at various temperatures, time-resolved measurements at various magnetic fields, and DCP measured for a dense and diluted sample #6; experimental data for additional CdSe/CdZnMnS samples (time-resolved measurements at various magnetic fields, DCP at various magnetic fields); TEM image of sample #4; modeling details: electron and hole penetration into shells, exchange interaction of charge carriers and excitons with Mn^{2+} ions, comment on anticrossing of exciton levels in a magnetic field, and comment on spin-dependent recombination (PDF)

■ AUTHOR INFORMATION

Corresponding Authors

Elena V. Shornikova − *Experimentelle Physik 2, Technische Universität Dortmund, 44227 Dortmund, Germany;* orcid.org/0000-0002-6866-9013; Email: elena.shornikova@tu-dortmund.de

Dmitri R. Yakovlev − *Experimentelle Physik 2, Technische Universität Dortmund, 44227 Dortmund, Germany;* orcid.org/0000-0001-7349-2745; Email: dmitri.yakovlev@tu-dortmund.de

Authors

Danil O. Tolmachev − *Experimentelle Physik 2, Technische Universität Dortmund, 44227 Dortmund, Germany;* orcid.org/0000-0002-7098-8515

Mikhail A. Prosnikov − *High Field Magnet Laboratory (HFML-EMFL), Radboud University, 6525 ED Nijmegen, The Netherlands;* orcid.org/0000-0002-7107-570X

Peter C. M. Christianen − *High Field Magnet Laboratory (HFML-EMFL), Radboud University, 6525 ED Nijmegen, The Netherlands;* orcid.org/0000-0002-6361-1605

Sushant Shendre − *LUMINOUS! Center of Excellence for Semiconductor Lighting and Displays, School of Electrical and Electronic Engineering, School of Physical and Materials Sciences, Nanyang Technological University, Singapore 639798, Singapore;* orcid.org/0000-0001-8586-7145

Furkan Isik − *LUMINOUS! Center of Excellence for Semiconductor Lighting and Displays, School of Electrical and Electronic Engineering, School of Physical and Materials Sciences, Nanyang Technological University, Singapore 639798, Singapore; Department of Electrical and Electronics Engineering, Department of Physics, UNAM − Institute of Materials Science and Nanotechnology, Bilkent University, 06800 Ankara, Turkey;* orcid.org/0000-0001-5881-5438

Savas Delikanli − *LUMINOUS! Center of Excellence for Semiconductor Lighting and Displays, School of Electrical and Electronic Engineering, School of Physical and Materials Sciences, Nanyang Technological University, Singapore 639798, Singapore; Department of Electrical and Electronics Engineering, Department of Physics, UNAM − Institute of Materials Science and Nanotechnology, Bilkent University, 06800 Ankara, Turkey;* orcid.org/0000-0002-0613-8014

Hilmi Volkan Demir − *LUMINOUS! Center of Excellence for Semiconductor Lighting and Displays, School of Electrical and Electronic Engineering, School of Physical and Materials Sciences, Nanyang Technological University, Singapore 639798, Singapore; Department of Electrical and Electronics Engineering, Department of Physics, UNAM − Institute of Materials Science and Nanotechnology, Bilkent University, 06800 Ankara, Turkey;* orcid.org/0000-0003-1793-112X

Manfred Bayer − *Experimentelle Physik 2 and Research Center FEMS, Technische Universität Dortmund, 44227 Dortmund, Germany;* orcid.org/0000-0002-0893-5949

Complete contact information is available at: https://pubs.acs.org/10.1021/acsanm.4c05364

Notes

The authors declare no competing financial interest.

https://doi.org/10.1021/acsanm.4c05364
ACS Appl. Nano Mater. 2025, 8, 974−984

■ ACKNOWLEDGMENTS

The authors thank A. V. Rodina and A. A. Golovatenko for discussions. The work of E.V.S. was funded by the Deutsche Forschungsgemeinschaft (DFG, German Research Foundation) − Project No.: 462009643. D.R.Y. and M.B. acknowledge support of the Deutsche Forschungsgemeinschaft in the frame of the International Collaborative Research Center TRR 160 (Project B1). The support of HFML-RU/NWO-I, a member of the European Magnetic Field Laboratory (EMFL), is acknowledged. H.V.D. gratefully acknowledges financial support in part from the Singapore Agency for Science, Technology and Research (A*STAR) MTC program under grant number M21J9b0085, Ministry of Education, Singapore, under its Academic Research Fund Tier 1 (MOE-RG62/20), and in part from TUBITAK 121C266 and 20AG001. H.V.D. also acknowledges support from TUBA and TUBITAK 2247-A National Leader Researchers Program (121C266).

■ REFERENCES

(1) Beaulac, R.; Archer, P. I.; Ochsenbein, S. T.; Gamelin, D. R. Mn^{2+}-doped CdSe quantum dots: new inorganic materials for spin-electronics and spin-photonics. *Adv. Funct. Mater.* **2008**, *18*, 3873.

(2) Bussian, D. A.; Crooker, S. A.; Yin, M.; Brynda, M.; Efros, A. L.; Klimov, V. I. Tunable magnetic exchange interactions in manganese-doped inverted core-shell ZnSe-CdSe nanocrystals. *Nat. Mater.* **2009**, *8*, 35.

(3) Norris, D. J.; Efros, A. L.; Erwin, S. C. Doped nanocrystals. *Science* **2008**, *319*, 1776.

(4) Pacuski, W.; Kossacki, P.; Ferrand, D.; Golnik, A.; Cibert, J.; Wegscheider, M.; Navarro-Quezada, A.; Bonanni, A.; Kiecana, M.; Sawicki, M.; Dietl, T. Observation of strong-coupling effects in a diluted magnetic semiconductor $Ga_{1-x}Fe_xN$. *Phys. Rev. Lett.* **2008**, *100*, No. 037204.

(5) Gaj, J. A.; Galazka, R. R.; Nawrocki, M. Giant exciton Faraday rotation in $Cd_{1-x}Mn_xTe$ mixed crystals. *Solid State Commun.* **1978**, *25*, 193.

(6) Golnik, A.; Ginter, J.; Gaj, J. A. Magnetic polarons in exciton luminescence of $Cd_{1-x}Mn_xTe$. *J. Phys. C* **1983**, *16*, 6073.

(7) Nawrocki, M.; Planel, R.; Fishman, G.; Galazka, R. Exchange-induced spin-flip raman scattering in a semimagnetic semiconductor. *Phys. Rev. Lett.* **1981**, *46*, 735.

(8) Yakovlev, D. R.; Ossau, W. Magnetic polarons. In: *Introduction to the physics of diluted magnetic semiconductors*; Kossut, J.; Gaj, J. A., Eds.; Springer-Verlag: Heidelberg, 2010; 221−262.

(9) Furdyna, J. K. Diluted magnetic semiconductors. *J. Appl. Phys.* **1988**, *64*, R29.

(10) *Diluted magnetic semiconductors*; Furdyna, J. K.; Kossut, J., Eds.; Academic Press: London, 1988.

(11) Dietl, T. Diluted magnetic semiconductors. In: *Handbook of Semiconductors*; Mahajan, S., Ed.; North-Holland: Amsterdam, 1994; *3b*, 1252.

(12) Gaj, J. A.; Kossut, J. Basic consequences of sp−d and d−d interactions in DMS. In: *Introduction to the physics of diluted magnetic Semiconductors*; Kossut, J.; Gaj, J. A., Eds.; Springer-Verlag: Heidelberg, 2010; 1−36.

(13) Merkulov, I. A.; Rodina, A. V. Exchange interaction between carriers and magnetic ions in quantum size heterostructures. In: *Introduction to the physics of diluted magnetic Semiconductors*; Kossut, J.; Gaj, J. A., Eds.; Springer-Verlag: Heidelberg, 2010; 65−102.

(14) Bryan, J. D.; Heald, S. M.; Chambers, S. A.; Gamelin, D. R. Strong room-temperature ferromagnetism in Co^{2+}-doped TiO_2 made from colloidal nanocrystals. *J. Am. Shem. Soc.* **2004**, *126*, 11640.

(15) Ochsenbein, S.; Feng, Y.; Whitaker, K.; Badaeva, E.; Liu, W. K.; Li, X.; Gamelin, D. R. Charge-controlled magnetism in colloidal doped semiconductor nanocrystals. *Nat. Nanotechnol.* **2009**, *4*, 681.

(16) Dietl, T.; Ohno, H. Dilute ferromagnetic semiconductors: Physics and spintronic structures. *Rev. Mod. Phys.* **2014**, *86*, 187.

(17) Kagan, C. R.; Bassett, L. C.; Murray, C. B.; Thompson, S. M. Colloidal quantum dots as platforms for quantum information science. *Chem. Rev.* **2021**, *121*, 3186.

(18) Rozhansky, I. V.; Mantsevich, V. N.; Maslova, N. S.; Arseyev, P. I.; Averkiev, N. S. Dynamic electron spin injection in semiconductor nanostructures. *J. Magn. Magn. Mater.* **2023**, *565*, No. 170303.

(19) Neumann, T.; Feldmann, S.; Moser, P.; Delhomme, A.; Zerhoch, J.; van de Goor, T.; Wang, S.; Dyksik, M.; Winkler, T.; Finley, J. J.; Plochocka, P.; Brandt, M. S.; Faugeras, C.; Stier, A. V.; Deschler, F. Manganese doping for enhanced magnetic brightening and circular polarization control of dark excitons in paramagnetic layered hybrid metal-halide perovskites. *Nat. Commun.* **2021**, *12*, 3489.

(20) Batista, E. A.; Silva, A. C. A.; Rezende, T. K. D. L.; Guimarães, E. V.; Pereira, P. A. G.; de Souza, P. E. N.; da Silva, R. S.; de Morais, P. C.; Dantas, N. O. Modulating the magnetic-optical properties of $Zn_{1-x}Co_xO$ nanocrystals with *x*-content. *J. Mater. Res.* **2021**, *36*, 1657.

(21) Reddy, L. H.; Arias, J. L.; Nicolas, J.; Couvreur, P. Magnetic nanoparticles: Design and characterization, toxicity and biocompatibility, pharmaceutical and biomedical applications. *Chem. Rev.* **2012**, *112*, 5818.

(22) Bruchez, M., Jr.; Moronne, M.; Gin, P.; Weiss, S.; Alivisatos, A. P. Semiconductor nanocrystals as fluorescent biological labels. *Science* **1998**, *281*, 2013.

(23) Chan, W. C. W.; Nie, S. Quantum dot bioconjugates for ultrasensitive nonisotopic detection. *Science* **1998**, *281*, 2016.

(24) Silva, T. G.; Moura, I. M. R.; Filho, P. E. C.; Pereira, M. I. A.; Filho, C. A. A.; Pereira, G.; Pereira, G. A. L.; Fontes, A.; Santos, B. S. ZnSe:Mn aqueous colloidal quantum dots for optical and biomedical applications. *Phys. Stat. Solidi C* **2016**, *13*, 530.

(25) Hoffman, D. M.; Meyer, B. K.; Ekimov, A. I.; Merkulov, I. A.; Efros, A. L.; Rosen, M.; Couino, G.; Gacoin, T.; Boilot, J. P. Giant internal magnetic fields in Mn doped nanocrystal quantum dots. *Solid State Commun.* **2000**, *114*, 547.

(26) Norris, D. J.; Yao, N.; Charnock, F. T.; Kennedy, T. A. High-quality nanganese-doped ZnSe nanocrystals. *Nano Lett.* **2001**, *1*, 3.

(27) Beaulac, R.; Archer, P. I.; Liu, X.; Lee, S.; Salley, G. M.; Dobrowolska, M.; Furdyna, J. K.; Gamelin, D. R. Spin-polarizable excitonic luminescence in colloidal Mn^{2+}-doped CdSe quantum dots. *Nano Lett.* **2008**, *8*, 1197.

(28) Turyanska, L.; Hill, R. J. A.; Makarovsky, O.; Moro, F.; Knott, A. N.; Larkin, O. J.; Patanè, A.; Meaney, A.; Christianen, P. C. M.; Fay, M. W.; Curry, R. J. Tuneable paramagnetic susceptibility and exciton g-factor in Mn-doped PbS colloidal nanocrystals. *Nanoscale* **2014**, *6*, 8919.

(29) Shornikova, E. V.; Yakovlev, D. R.; Tolmachev, D. O.; Ivanov, V. Yu.; Kalitukha, I. V.; Sapega, V. F.; Kudlacik, D.; Kusrayev, Yu. G.; Golovatenko, A. A.; Shendre, S.; Delikanli, S.; Demir, H. V.; Bayer, M. Magneto-optics of excitons interacting with magnetic ions in CdSe/CdMnS colloidal nanoplatelets. *ACS Nano* **2020**, *14*, 9032.

(30) Halder, O.; Mallik, G.; Suffczyński, J.; Pacuski, W.; Varadwaj, K. S. K.; Satpati, B.; Rath, S. Enhanced exciton binding energy, Zeeman splitting and spin polarization in hybrid layered nanosheets comprised of (Cd, Mn)Se and nitrogen-doped graphene oxide: Implication for semiconductor devices. *Nanotechnol.* **2021**, *32*, 325204.

(31) Strassberg, R.; Delikanli, S.; Barak, Y.; Dehnel, J.; Kostadinov, A.; Maikov, G.; Hernandez-Martinez, P. L.; Sharma, M.; Demir, H. V.; Lifshitz, E. Persuasive evidence for electron-nuclear coupling in diluted magnetic colloidal nanoplatelets using optically detected magnetic resonance spectroscopy. *J. Phys. Chem. Lett.* **2019**, *10*, 4437.

(32) Tolmachev, D. O.; Ivanov, V. Yu; Yakovlev, D. R.; Shornikova, E. V.; Witkowski, B.; Shendre, S.; Isik, F.; Delikani, S.; Demir, H. V.; Bayer, M. Optically detected magnetic resonance in CdSe/CdMnS nanoplatelets. *Nanoscale* **2020**, *12*, 21932.

(33) Dehnel, J.; Barak, Y.; Meir, I.; Budniak, A. K.; Nagvenkar, A. P.; Gamelin, D. R.; Lifshitz, E. Insight into the spin properties in undoped and Mn-doped CdSe/CdS-seeded nanorods by optically detected magnetic resonance. *ACS Nano* **2020**, *14*, 13478.

https://doi.org/10.1021/acsanm.4c05364
ACS Appl. Nano Mater. 2025, 8, 974−984

(34) Babunts, R. A.; Uspenskaya, Yu. A.; Romanov, N. G.; Orlinskii, S. B.; Mamin, G. V.; Shornikova, E. V.; Yakovlev, D. R.; Bayer, M.; Isik, F.; Shendre, S.; Delikanli, S.; Demir, H. V.; Baranov, P. G. High-frequency EPR and ENDOR spectroscopy of Mn^{2+} ions in CdSe/CdMnS nanoplatelets. *ACS Nano* **2023**, *17*, 4474.
(35) Beaulac, R.; Schneider, L.; Archer, P. I.; Bacher, G.; Gamelin, D. R. Light-induced spontaneous magnetization in doped colloidal quantum dots. *Science* **2009**, *325*, 973.
(36) Rice, W. D.; Liu, W.; Pinchetti, V.; Yakovlev, D. R.; Klimov, V. I.; Crooker, S. A. Direct measurements of magnetic polarons in $Cd_{1-x}Mn_xSe$ nanocrystals from resonant photoluminescence. *Nano Lett.* **2017**, *17*, 3068.
(37) Rice, W. D.; Liu, W.; Baker, T. A.; Sinitsyn, N. A.; Klimov, V. I.; Crooker, S. A. Revealing giant internal magnetic fields due to spin fluctuations in magnetically doped colloidal nanocrystals. *Nat. Nanotechnol.* **2016**, *11*, 137.
(38) Diroll, B. T.; Guzelturk, B.; Po, H.; Dabard, C.; Fu, N.; Makke, L.; Lhuillier, E.; Ithurria, S. 2D II−VI semiconductor nanoplatelets: from material synthesis to optoelectronic integration. *Chem. Rev.* **2023**, *123*, 3543.
(39) Ithurria, S.; Tessier, M. D.; Mahler, B.; Lobo, R. P. S. M.; Dubertret, B.; Efros, Al L. Colloidal Nanoplatelets with two-dimensional electronic structure. *Nat. Mater.* **2011**, *10*, 936.
(40) Ithurria, S.; Talapin, D. V. Colloidal atomic layer deposition (c-ALD) using self-limiting reactions at nanocrystal surface coupled to phase transfer between polar and nonpolar media. *J. Am. Chem. Soc.* **2012**, *134*, 18585.
(41) Biadala, L.; Liu, F.; Tessier, M. D.; Yakovlev, D. R.; Dubertret, B.; Bayer, M. Recombination dynamics of band edge excitons in quasi-two-dimensional CdSe nanoplatelets. *Nano Lett.* **2014**, *14*, 1134.
(42) Delikanli, S.; Akgul, M. Z.; Murphy, J. R.; Barman, B.; Tsai, Y.; Scrace, T.; Zhang, P.; Bozok, B.; Hernández-Martínez, P. L.; Christodoulides, J.; Cartwright, A. N.; Petrou, A.; Demir, H. V. Mn^{2+}-doped CdSe/CdS core/multishell colloidal quantum wells enabling tunable carrier-dopant exchange interactions. *ACS Nano* **2015**, *9*, 12473.
(43) Morgan, D. P.; Kelley, D. F. Exciton localization and radiative lifetimes in CdSe nanoplatelets. *J. Phys. Chem. C* **2019**, *123*, 18665.
(44) Peng, L.; Otten, M.; Hazarika, A.; Coropceanu, I.; Cygorek, M.; Wiederrecht, G. P.; Hawrylak, P.; Talapin, D. V.; Ma, X. Bright trion emission from semiconductor nanoplatelets. *Phys. Rev. Mater.* **2020**, *4*, No. 056006.
(45) Geiregat, P.; Rodá, C.; Tanghe, I.; Singh, S.; Di Giacomo, A.; Lebrun, D.; Grimaldi, G.; Maes, J.; Van Thourhout, D.; Moreels, I.; Houtepen, A. J.; Hens, Z. Localization-limited exciton oscillator strength in colloidal CdSe nanoplatelets revealed by the optically induced stark effect. *Light Sci. Appl.* **2021**, *10*, 112.
(46) Curti, L.; Dabard, C.; Makké, L.; Fu, N.; Lehouelleur, H.; Hua, M.; Bossavit, E.; Cavallo, M.; Xu, X. Z.; Pierucci, D.; Silly, M. G.; Guzelturk, B.; Lhuillier, E.; Climente, J. I.; Diroll, B. T.; Ithurria, S. Lateral confinement in 2D nanoplatelets: A strategy to expand the colloidal quantum engineering toolbox. *Adv. Opt. Mater.* **2024**, *12*, No. 2400555.
(47) Chang, W. J.; Zeng, H.; Terry Weatherly, C. K.; Provazza, J.; Liu, P.; Weiss, E. A.; Stern, N. P.; Tempelaar, R. Dark state concentration dependent emission and dynamics of CdSe nanoplatelet exciton-polaritons. *ACS Nano* **2024**, *18*, 20226.
(48) Swift, M. W.; Efros, A. L.; Erwin, S. C. Controlling light emission from semiconductor nanoplatelets using surface chemistry. *Nat. Commun.* **2024**, *15*, 7737.
(49) Murphy, J. R.; Delikanli, S.; Scrace, T.; Zhang, P.; Norden, T.; Thomay, T.; Cartwright, A. N.; Demir, H. V.; Petrou, A. Time-resolved photoluminescence study of CdSe/CdMnS/CdS core/multi-shell nanoplatelets. *Appl. Phys. Lett.* **2016**, *108*, 242406.
(50) Muckel, F.; Delikanli, S.; Hernandez-Martinez, P. L.; Priesner, T.; Lorenz, S.; Ackermann, J.; Sharma, M.; Demir, H. V.; Bacher, G. sp−d exchange interactions in wave function engineered colloidal CdSe/Mn:CdS hetero-nanoplatelets. *Nano Lett.* **2018**, *18*, 2047.
(51) Davis, A. H.; Hofman, E.; Chen, K.; Li, Z.-J.; Khammang, A.; Zamani, H.; Franck, J. M.; Maye, M. M.; Meulenberg, R. W.; Zheng, W. Exciton energy shifts and tunable dopant emission in manganese-doped two-dimensional CdS/ZnS core/shell nanoplatelets. *Chem. Mater.* **2019**, *31*, 2516.
(52) Shabani, F.; Ahmad, M.; Kumar, S.; Delikanli, S.; Isik, F.; Bhattacharya, A.; Petrou, A.; Demir, H. V. Thermodynamic silver doping of core/shell colloidal quantum wells imparted with paramagnetic properties emitting at near-infrared. *Chem. Mater.* **2023**, *35*, 4159.
(53) Viswanatha, R.; Pietryga, J. M.; Klimov, V. I.; Crooker, S. A. Spin-polarized Mn^{2+} emission from Mn-doped colloidal nanocrystals. *Phys. Rev. Lett.* **2011**, *107*, No. 067402.
(54) Yang, Y.; Chen, O.; Angerhofer, A.; Cao, Y. C. On doping CdS/ZnS core/shell nanocrystals with Mn. *J. Am. Chem. Soc.* **2008**, *130*, 15649.
(55) Pradhan, N.; Das Adhikari, S.; Nag, A.; Sarma, D. D. Luminescence, plasmonic, and magnetic properties of doped semiconductor nanocrystals. *Angew. Chem., Int. Ed. Engl.* **2017**, *56*, 7038.
(56) Dai, L.; Strelow, C.; Lesyuk, R.; Klinke, C.; Kipp, T.; Mews, A. Mn^{2+}-doped ZnSe/ZnS core/shell nanoplatelets as low-toxic UV-to-Vis light-converters with enhanced optical properties. *ACS Appl. Nano Mater.* **2023**, *6*, 11124.
(57) Nelson, H. D.; Bradshaw, L. R.; Barrows, C. J.; Vlaskin, V. A.; Gamelin, D. R. Picosecond dynamics of excitonic magnetic polarons in colloidal diffusion-doped $Cd_{1-x}Mn_xSe$ quantum dots. *ACS Nano* **2015**, *9*, 11177.
(58) Delikanli, S.; Yu, G.; Yeltik, A.; Bose, S.; Erdem, T.; Yu, J.; Erdem, O.; Sharma, M.; Sharma, V. K.; Quliyeva, U.; Shendre, S.; Dang, C.; Zhang, D. H.; Sum, T. C.; Fan, W.; Demir, H. V. Ultrathin highly luminescent two-monolayer colloidal CdSe nanoplatelets. *Adv. Funct. Mater.* **2019**, *29*, No. 1901028.
(59) Shendre, S.; Delikanli, S.; Li, M.; Dede, D.; Pan, Z.; Ha, S. T.; Fu, Y. H.; Hernández-Martínez, P. L.; Yu, J.; Erdem, O.; Kuznetsov, A. I.; Dang, C.; Sum, T. C.; Demir, H. V. Ultrahigh-efficiency aqueous flat nanocrystals of CdSe/CdS@$Cd_{1-x}Zn_xS$ colloidal core/crown@alloyed-shell quantum wells. *Nanoscale* **2019**, *11*, 301.
(60) Antolinez, F. V.; Rabouw, F. T.; Rossinelli, A. A.; Cui, J.; Norris, D. J. Observation of electron shakeup in CdSe/CdS core/shell nanoplatelets. *Nano Lett.* **2019**, *19*, 8495.
(61) Llusar, J.; Climente, J. I. Nature and control of shakeup processes in colloidal nanoplatelets. *ACS Photonics* **2020**, *7*, 3086.
(62) Efros, A. L.; Rosen, M.; Kuno, M.; Nirmal, M.; Norris, D. J.; Bawendi, M. Band-edge exciton in quantum dots of semiconductors with a degenerate valence band: dark and bright exciton states. *Phys. Rev. B* **1996**, *54*, 4843.
(63) Shornikova, E. V.; Biadala, L.; Yakovlev, D. R.; Sapega, V. F.; Kusrayev, Yu. G.; Mitioglu, A. A.; Ballottin, M. V.; Christianen, P. C. M.; Belykh, V. V.; Kochiev, M. V.; Sibeldin, N. N.; Golovatenko, A. A.; Rodina, A. V.; Gippius, N. A.; Kuntzmann, A.; Jiang, Y.; Nasilowski, M.; Dubertet, B.; Bayer, M. Addressing the exciton fine structure in colloidal nanocrystals: the case of CdSe nanoplatelets. *Nanoscale* **2018**, *10*, 646−656.
(64) Smirnova, O. O.; Kalitukha, I. V.; Rodina, A. V.; Dimitriev, G. S.; Sapega, V. F.; Ken, O. S.; Korenev, V. L.; Kozyrev, N. V.; Nekrasov, S. V.; Kusrayev, Y. G.; Yakovlev, D. R.; Dubertret, B.; Bayer, M. Optical alignment and optical orientation of excitons in CdSe/CdS colloidal nanoplatelets. *Nanomaterials* **2023**, *13*, 2402.
(65) Johnston-Halperin, E.; Awschalom, D. D.; Crooker, S. A.; Efros, A. L.; Rosen, M.; Peng, X.; Alivisatos, A. P. Spin spectroscopy of dark excitons in CdSe quantum dots to 60 T. *Phys. Rev. B* **2001**, *63*, No. 205309.
(66) Biadala, L.; Louyer, Y.; Tamarat, Ph.; Lounis, B. Direct observation of the two lowest exciton zero-phonon lines in single CdSe/ZnS nanocrystals. *Phys. Rev. Lett.* **2009**, *103*, No. 037404.
(67) Shornikova, E. V.; Yakovlev, D. R.; Biadala, L.; Crooker, S. A.; Belykh, V. V.; Kochiev, M. V.; Kuntzmann, A.; Nasilowski, M.;

https://doi.org/10.1021/acsanm.4c05364
ACS Appl. Nano Mater. 2025, 8, 974−984

Dubertet, B.; Bayer, M. Negatively charged excitons in CdSe nanoplatelets. *Nano Lett.* **2020**, *20*, 1370−1377.
(68) Granados del Águila, A.; Pettinari, G.; Groeneveld, E.; de Mello Donegá, C.; Vanmaekelbergh, D.; Maan, J. C.; Christianen, P. C. M. Optical spectroscopy of dark and bright excitons in CdSe nanocrystals in high magnetic fields. *J. Phys. Chem. C* **2017**, *121*, 23693.
(69) Qiang, G.; Golovatenko, A. A.; Shornikova, E. V.; Yakovlev, D. R.; Rodina, A. V.; Zhukov, E. A.; Kalitukha, I. V.; Sapega, V. F.; Kaibyshev, V. Kh.; Prosnikov, M. A.; Christianen, P. C. M.; Onushchenko, A. A.; Bayer, M. Polarized emission of CdSe nanocrystals in magnetic field: the role of phonon-assisted recombination of the dark exciton. *Nanoscale* **2021**, *13*, 790.
(70) Shornikova, E. V.; Biadala, L.; Yakovlev, D. R.; Feng, D.; Sapega, V. F.; Flipo, N.; Golovatenko, A. A.; Semina, M. A.; Rodina, A. V.; Mitioglu, A. A.; Ballottin, M. V.; Christianen, P. C. M.; Kusrayev, Yu. G.; Nasilowski, M.; Dubertret, B.; Bayer, M. Electron and hole g-factors and spin dynamics of negatively charged excitons in CdSe/CdS colloidal nanoplatelets with thick shells. *Nano Lett.* **2018**, *18*, 373.
(71) Efros, A. L. Fine structure and polarization properties of band-edge excitons in semiconductor nanocrystals. In *Semiconductor and metal nanocrystals: synthesis and electronic and optical properties*; Klimov, V. I., Ed.; Dekker: New York, 2003; 103.
(72) Shornikova, E. V.; Golovatenko, A. A.; Yakovlev, D. R.; Rodina, A. V.; Biadala, L.; Qiang, G.; Kuntzmann, A.; Nasilowski, M.; Dubertret, B.; Polovitsyn, A.; Moreels, I.; Bayer, M. Surface spin magnetism controls the polarized exciton emission from CdSe nanoplatelets. *Nat. Nanotechnol.* **2020**, *15*, 277.
(73) Semina, M. A.; Golovatenko, A. A.; Rodina, A. V. Influence of the spin-orbit split-off valence band on the hole *g* factor in semiconductor nanocrystals. *Phys. Rev. B* **2021**, *104*, No. 205423.
(74) Kudlacik, D.; Sapega, V. F.; Yakovlev, D. R.; Kalitukha, I. V.; Shornikova, E. V.; Rodina, A. V.; Ivchenko, E. L.; Dimitriev, G. S.; Nasilowski, M.; Dubertet, B.; Bayer, M. Single and double electron spin-flip raman scattering in CdSe colloidal nanoplatelets. *Nano Lett.* **2020**, *20*, 517−525.
(75) Feng, D.; Yakovlev, D. R.; Dubertet, B.; Bayer, M. Charge separation dynamics in CdSe/CdS core/shell nanoplatelets addressed by coherent electron spin precession. *ACS Nano* **2020**, *14*, 7237−7244.
(76) Ivchenko, E. L. Magnetic circular polarization of exciton photoluminescence. *Phys. Solid State* **2018**, *60*, 1514.
(77) Liu, F.; Rodina, A. V.; Yakovlev, D. R.; Greilich, A.; Golovatenko, A. A.; Susha, A. S.; Rogach, A. L.; Kusrayev, Y. G.; Bayer, M. Exciton spin dynamics of colloidal CdTe nanocrystals in magnetic fields. *Phys. Rev. B* **2014**, *89*, No. 115306.
(78) Rodina, A. V.; Efros, Al. L. Radiative recombination from dark excitons in nanocrystals: activation mechanisms and polarization properties. *Phys. Rev. B* **2016**, *93*, No. 155427.
(79) Feng, F.; NGuyen, L. T.; Nasilowski, M.; Nadal, B.; Dubertret, B.; Maître, A.; Coolen, L. Probing the fluorescence dipoles of single cubic CdSe/CdS nanoplatelets with vertical or horizontal orientations. *ACS Photonics* **2018**, *5*, 1994.

https://doi.org/10.1021/acsanm.4c05364
ACS Appl. Nano Mater. 2025, 8, 974−984